CrossMark

Pull-Out Behaviour of Hooked End Steel Fibres Embedded in Ultra-high Performance Mortar with Various W/B Ratios

Sadoon Abdallah, Mizi Fan*, and Xiangming Zhou

Abstract: This paper presents the fibre-matrix interfacial properties of hooked end steel fibres embedded in ultra-high performance mortars with various water/binder (W/B) ratios. The principle objective was to improve bond behaviour in terms of bond strength by reducing the (W/B) ratio to a minimum. Results show that a decrease in W/B ratio has a significant effect on the bond-slip behaviour of both types of 3D fibres, especially when the W/B ratio was reduced from 0.25 to 0.15. Furthermore, the optimization in maximizing pullout load and total pullout work is found to be more prominent for the 3D fibres with a larger diameter than for fibres with a smaller diameter. On the contrary, increasing the embedded length of the 3D fibres did not result in an improvement on the maximum pullout load, but increase in the total pullout work.

Keywords: pullout behaviour, bond mechanisms, water/binder ratio, hook geometry, embedment length and fibre-matrix interface.

1. Introduction

Nowadays one of the main challenges that the concrete industry facing; is how to improve the tensile strength and durability of mortar and concrete (Petrone et al. 2016; Alberti et al. 2014). The addition of randomised short fibres into mortar has shown to be capable of controlling crack progression as well as resisting tensile stresses (Adjrad et al 2016; Hwang et al. 2016; El-Mal et al. 2015; Sorensen et al. 2014; Islam and Alam 2013a, b; Romualdi et al. 1968). The efficiency of fibres in transferring applied stresses is greatly dependent on the fibre-matrix interface properties of fibre reinforced concrete (FRC) (Abdallah et al. 2016; Dinh et al. 2016; Lu et al. 2016; Tadepalli et al. 2015). Therefore, the bond-slip characteristics play a crucial role in controlling the tensile behaviour of FRC (Li and Liu 2016; Srikar et al. 2016; Bentur et al. 1995).

To improve the bonding strength of fibre and matrix interfaces, a number of modifications may be adopted. The densification of interfacial transition zone (ITZ) (Chan and Li 1997) by (a) increasing the fineness of materials particles (Wille and Naaman 2013), (b) reducing water/binder ratio (W/B) (Beglarigale and Yazıcı 2015; Beygi et al. 2013; Markovic 2006), (c) using pozzolanic materials such silica fume and quartz powder (Shaikh et al. 2016; Abbas et al.

2016; Chan and Chu 2004), (d) optimising surface properties through chemical treatment to increase adhesion or enhance surface roughness (Wille and Naaman 2013) and use of deformed fibres, such as corrugated fibre and hooked end fibre is a very efficient in improving bond properties and mechanical properties due to mechanical anchorage (Wu et al. 2016; Wille and Naaman 2012). One of the most recommended methods to investigate the bond characteristics is through single fibre pullout test (Laranjeira de Oliveira 2010). The test configuration is able to simulate the realistic case of cracking bridging by fibres in a FRC element (joo Kim, 2009). These test results could provide a comprehensive understanding on bond-slip characteristics and enable further improvement to fibre-matrix interfacial properties (Wille and Naaman 2010).

Ultra-high performance concrete (UHPC) mainly consists of very fine materials (less than 0.5 mm) and is designated to generate compressive strength exceeding 150 MPa (Yoo and Yoon, 2016; Shi et al. 2015; Wang et al. 2015; Wille et al. 2014). Research concerned with incorporating various types of steel fibres in UHPC has raised significantly interests due to its ability to achieve ductile behaviour under tension (Lim and Hong 2016; Abdallah et al. 2016; Kang et al. 2016; Wille et al. 2014; Lee et al. 2010). Yet, for the same ingredients of UHPC a significant difference in compressive strength can be found due to different W/B ratio (Torregrosa 2014). The great effect of W/B ratio on concrete performance may arise as a result of controlling the capillary pores which lead to increased concrete strength (Torregrosa 2014).

Although numerous researches has been conducted to investigate the pullout behaviour of steel fibres embedded in UHPC matrix, research in the optimization of bond characteristics of UHPC is limited (Wille and Naaman 2012).

Civil Engineering, College of Engineering, Design and Physical Sciences, Brunel University London, Uxbridge, Middlesex UB8 3PH, UK.
*Corresponding Author; E-mail: mizi.fan@brunel.ac.uk

Optimising the fibre-matrix bond characteristics in terms of bond strength is the key parameter that enhances the tensile response of UHP-FRC composites (Abdallah et al. 2016; Cunha 2010). To further achieve the effect of fibre-matrix properties on pullout behaviour, the quality of ultra-high performance matrix could be improved by lowering W/B ratio.

The objectives of this research are first to understand the mechanisms of interfacial bonding and bond-slip characteristics of UHP-FRC composites through a comprehensive determination of the influence of various parameters, such as fibre diameter and embedded length. The research is then aimed at further reducing W/B ratio to a minimum (i.e. <0.2) and investigating its effect on pull-out behaviour with taking into account the workability and rheological properties of the fresh mixture.

2. Experimental Programme

2.1 Materials

The ultra-high performance fibre reinforced mortar matrix (UHP-FRM) with different W/B ratio (W/B = 0.15, 0.20 and 0.25) considered here is produced by the following ingredients: Portland cement CEM III 52.5 N confirming to BS EN 197-1; densified silica fume; fine sand (150–600) micrometres (μm); ground quartz with average particle size (10 μm); superplasticizer (TamCem23SSR), accelerator (203 accelerator and frostproofer) and water. The mix proportion adopted in this study is summarized in Table 1. Two types of commercially available and commonly used 3Dramix hooked-end steel fibres (3DH) were used to reinforce the UHPM (Table 2). The geometrical properties of each fibre type are depicted in Fig. 1 and detailed in Table 2. For each type of fibre, the fibres were electronically scanned and measurements of the end-hook geometry were acquired using the electron microscope (SUPRA 35 VP) (Fig. 2).

2.2 Sample Preparation

The pull-out test specimens prepared were cylinders with a diameter of 100 mm and height of 50 mm. In each test specimen, a single steel fibre was carefully placed through a hole

which was made in the bottom of moulds (Fig. 3). Three different embedded lengths L_E (10, 15 and 30 mm) were investigated in this study. For compressive strength test three cubes of (100 × 100 × 100 mm) were prepared for each mixture differentiated in W/B ratio. During mortar fabrication, the components were firstly dry mixed for approximately 1 min followed by the addition of water and superplasticizer to the dry mixture, which were then mixed for 11 min. After casting and vibration, the specimens were covered with a thin polyethylene film and left for 24 h at room temperature. Then specimens were removed from their moulds and cured for a further 28 days in a conditioning chamber (20 ± 2 °C, 96 ± 4% RH). The free end of the steel fibre for the pullout specimens was covered with an anti-rust coating to prevent the corrosion during the curing to occur. For all series, the test was carried out at an age of 30 ± 2 days and the average of three specimens was adopted.

2.3 Test Setup

The pull-out tests were performed using a specially designed grip system, as illustrated in Fig. 4, which was attached to an Instron 5584 universal testing machine. The grips were designed such that the forces applied to the fibre provided a true reflection of the real situation experienced by fibres bridging a crack. The body of the gripping system was machined in a lathe using mild steel and had a tapered end to allow the insertion of four M4 grub screws (Fig. 4). These were then tightened around the steel fibre to an equal torque to ensure an even distribution of gripping pressure and to minimise deformation or breakage of the fibre ends. Two linear variable differential transformer (LVDT) transducers were used to measure the distance travelled by the steel fibre relative to the concrete face during testing (i.e. the pull-out distance). They were held in place using aluminium sleeves on either side of the main grip body (Fig. 4). The LVDTs had ball bearings at the tips to allow for accurate readings on the face of the samples. The sample was secured to the Instron base using clamps with riser blocks and M16 studs. The specimen was positioned on a brass round disc to remove any discrepancies in the sample base and allow for distortion. In all pull-out tests, a displacement rate of 10 μm/s was adopted.

Table 1 Constituents and proportions of ultra-high performance mortars (kg/m³).

Type	UHPM1	UHPM2	UHPM3
Constituent		Kg/m³	
Cement type III 52.5 N	710	710	710
Silica fume	231	231	231
Ground quratz	211	211	211
Fine sand	1020	1020	1020
Superplasticizer	30.7	30.7	30.7
Accelerator	30	30	30
Water	140.7	186.7	243.7
W/B	0.15	0.20	0.25

Table 2 General properties of hooked end steel fibres.

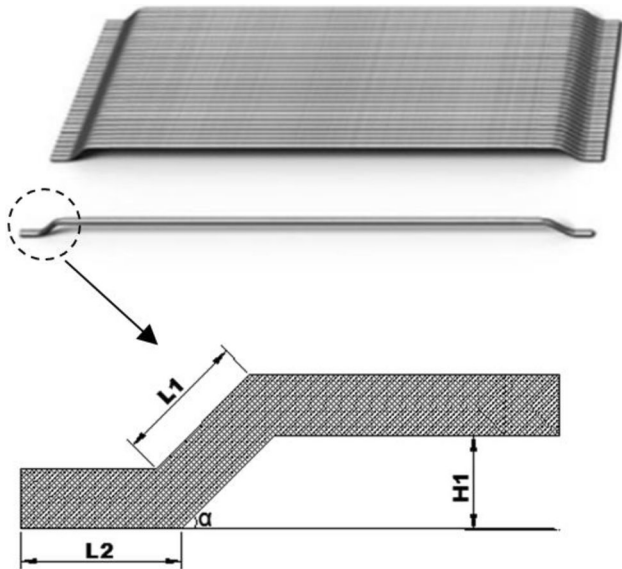| Fibre type	Lf (mm)	Df (mm)	Lf/Df	L1 (mm)	L2 (mm)	α (°)	H1 (mm)	Tensile strength (MPa)
3DH1	35	0.55	65	2.55	2.22	38.3	1.85	1345
3DH2	60	0.90	65	2.12	2.95	45.7	1.77	1160

Fig. 1 Geometrical properties of hooked end fibres.
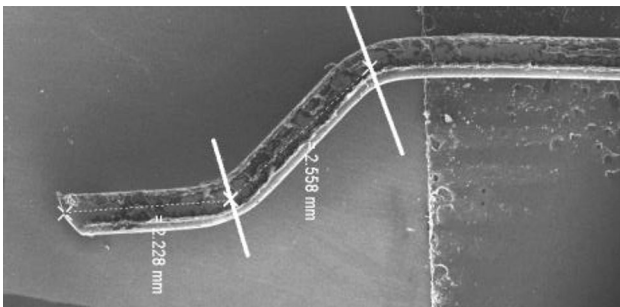
Fig. 2 SEM image shows measuring the hook dimensions.

2.4 Theoretical Consideration of σ_{max}, τ_{av} and τ_{eq}

In order to assess and compare the pullout behaviour of the two types of hooked end steel fibres embedded in different ultra-high performance mortars (UHPMs), the following parameters are considered based on the experimental results (Wille and Naaman 2012):

- Maximum fibre tensile stress, σ_{max} that can be obtained by dividing the maximum pullout load, P_{max} over nominal cross-sectional area of the fibre, A_f.

$$\sigma_{max} = \frac{P_{max}}{A_f} \tag{1}$$

Average bond strength, τ_{av}, can be defined as the maximum pullout load based on the initial embedment length surface area (Wille and Naaman 2013).

$$\tau_{av} = \frac{P_{max}}{\pi \times d_f \times L_E} \tag{2}$$

where τ_{av} is the average bond strength, P_{max} is the maximum pullout load, d_f is the fibre diameter, and L_E is the embedment length of steel fibre.

Equivalent bond strength, τ_{eq} can be defined as the average bond strength based on the total pullout work during the entire fibre pullout (joo Kim 2009).

$$\tau_{eq} = \frac{2 \times W_P}{\pi \times d_f \times L_E^2} \tag{3}$$

where τ_{eq} is the equivalent bond strength, W_p is the total pullout work, d_f is the fibre diameter, and L_E is the embedment length of steel fibre.
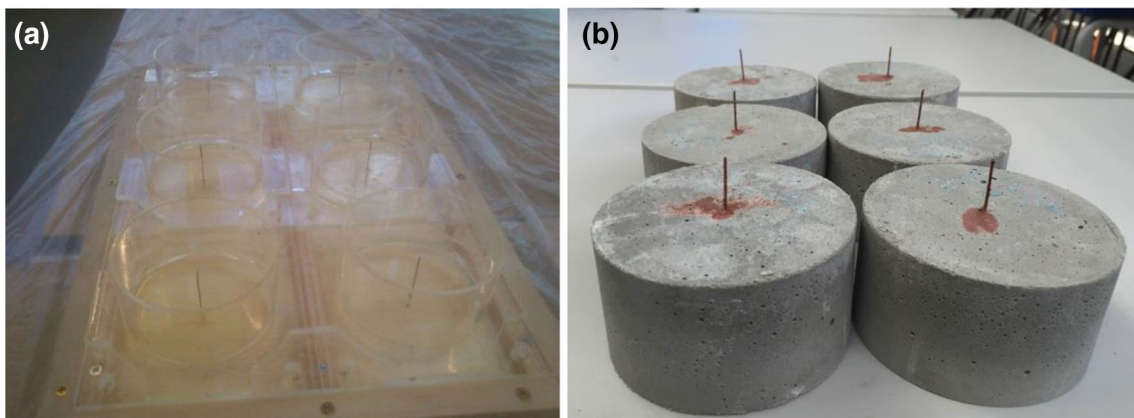

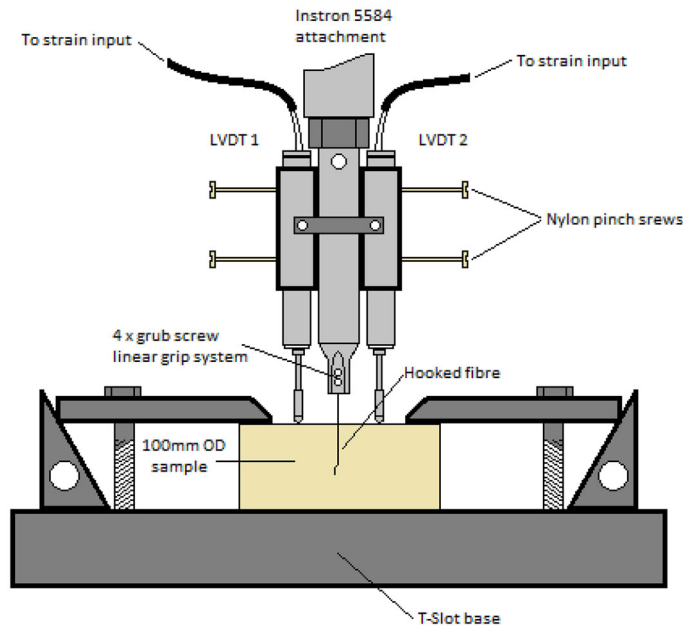**Fig. 3** Single fiber pullout moulds and specimens. **a** Moulds, **b** specimens.

Fig. 4 Pull-out test setup.

3. Results and Discussion

3.1 Fresh and Hardened Properties of UHPMs

To evaluate the workability and rheological properties of fresh mortars, the slump-flow test according to EN 12350-8:2010 (2010) were performed. It can be seen from Table 3 that all UHPMs mixtures had excellent rheological and self-compacting properties (Fig. 5). However, the reducing of W/B ratio leads to a decrease in slump-flow diameter (SFD), while time to reach 500 mm spread (T_{500}) is increased. This is in agreement with other results reported by (Deeb et al. 2012). The average compressive strength was remarkably enhanced for all UHPMs by decreasing W/B ratio (Table 3). This indicates that an excessive water in the matrix may result in adverse effect on the formulation of microstructure and hence the property of the concrete.

3.2 Effect of Water/Binder Ratio on Pullout Behaviour

The average pullout load-slip curves of the two types of 3D hooked end steel fibres embedded in ultra-high performance mortar matrix with three different water/binder ratios (W/B = 0.15, 0.20, 0.25) are presented in Figs. 6 and 7. The maximum pullout load and the total pullout work (the area under the pullout curve) of both types of hooked end fibres increase as the W/B ratio decreases (Table 4). It can also be seen from the curves that decreasing W/B ratio from 0.25 to 0.15 remarkably enhances the maximum pullout load and pullout work. However, for 3DH1 fibre with L_E (15 mm) and
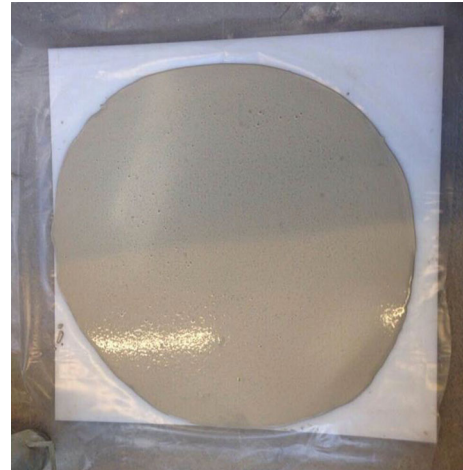

Fig. 5 Slump flow test of UHPM1.

Table 3 Properties of fresh and hardened UHPMs.

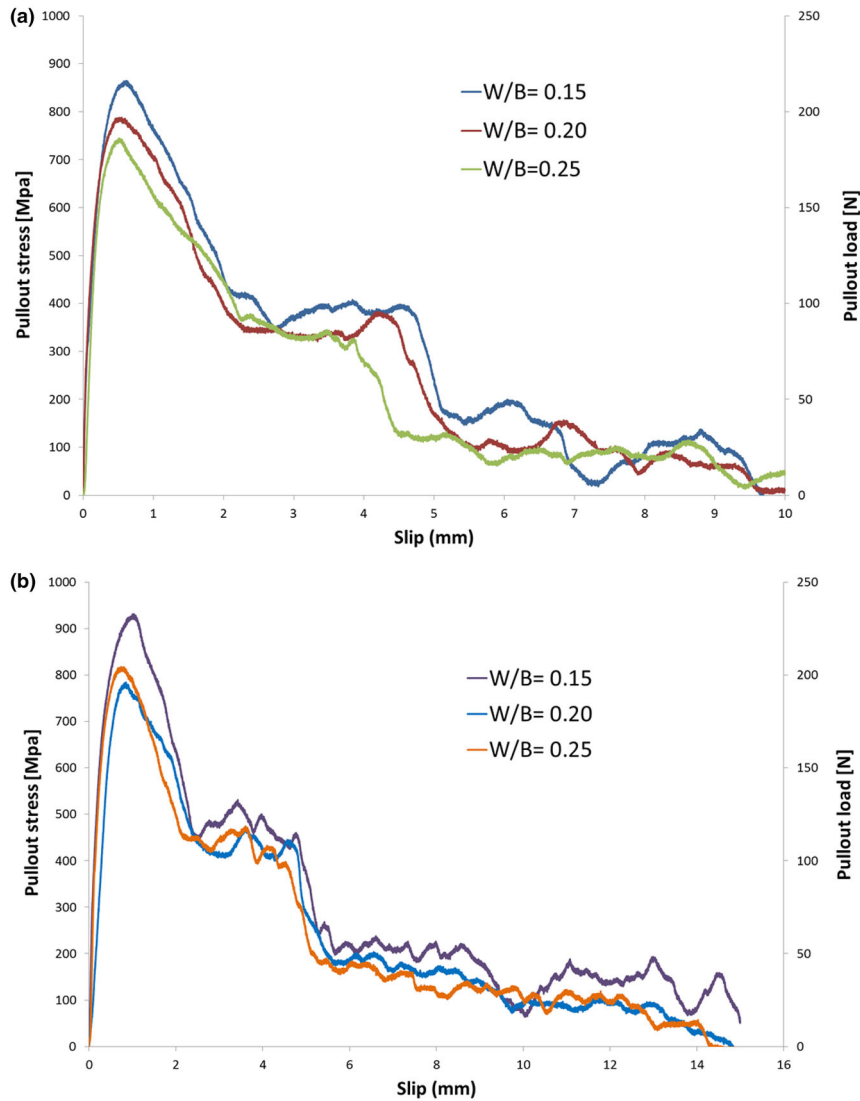| Mixtures	Slump flow test		Density	$f^*_{cm,28d}$ (MPa)
	$T_{500\ (S)}$	SFD(mm)	(kg/m^3)	
UHPM1	6	780	2497	178
UHPM2	4	850	2485	152
UHPM3	3	910	2464	149

* Average of three specimens.

Fig. 6 Average pullout load–slip curves of 3DH1 fibres. **a** Embedded length (10 mm), **b** embedded length (16 mm).

3DH2 fibre with L_E (30 mm) a slight difference in pullout behaviour is observed when W/B ratio decreased from 0.25 to 0.20. The high compressive strength associated with 0.15 W/B ratio ($f_c = 172$ MPa) and the close compressive strengths for 0.20 W/B ratio ($f_c = 152$ MPa) and 0.25 W/B ratio ($f_c = 149$ MPa) can interpret the better pullout behaviour of the specimens with 0.15 W/B ratio and the similar behaviour of the specimens with 0.20 W/B and 0.25 W/B ratios.

On the other hand, the pullout response of both types of fibres exhibit somewhat different slip behaviour before the second drop of the pullout load. As can be seen in Figs. 6 and 7, the slip capacity of both fibres noticeably increases when W/B ratio decreases. It has been found that the decease of W/B ratio not only increases the maximum pullout load but also effectively enhances the Δ_{peak} (Table 4). This effect may be attributed to the significant improvement in the fibre-matrix interfacial properties in term of bond strength. Furthermore, a significant difference in the total pullout work can be observed due to different slip capacities.

For the 3DH2 fibre with embedded length of 10 mm, the maximum pullout load is increased by 38.88%, while the

corresponding increase for 3DH1 fibre is only 16.75%, when W/B ratio decreased from 0.25 to 0.15. In contrast, the decrease of W/B ratio from 0.25 to 0.20 the maximum pullout load of the 3DH2 fibre with embedded length of 30 mm is only increased by 1.41%, while for the 3DH1 fibre with embedded length of 15 mm it is decreased by 4.41%. This indicates that the decrease W/B ratio from 0.25 to 0.20 does not offer any improvement in maximum pullout load. On the other hand, the improvement in total pullout work due to decrease in W/B ratio is relatively more significant than that in maximum pullout load for both types of fibres with L_E (10 mm). The total pullout work is increased by 52.11 and 25.9% for 3DH2 and 3DH1 fibres, respectively when W/B decreased from 0.25 to 0.15 (Table 4). These results are directly related to significant improvement in bond strength which increases the consumed energy during the pullout process. Beglarigale et al. (Beglarigale and Yazıcı 2015) have also reported the similar results. It has been found that increasing the W/B ratio of the reactive powder concrete (RPC) mixture from 0.2 to 0.3, 0.4, 0.5, and 0.6, leads to decrease the maximum pull-out load values by 0–8,
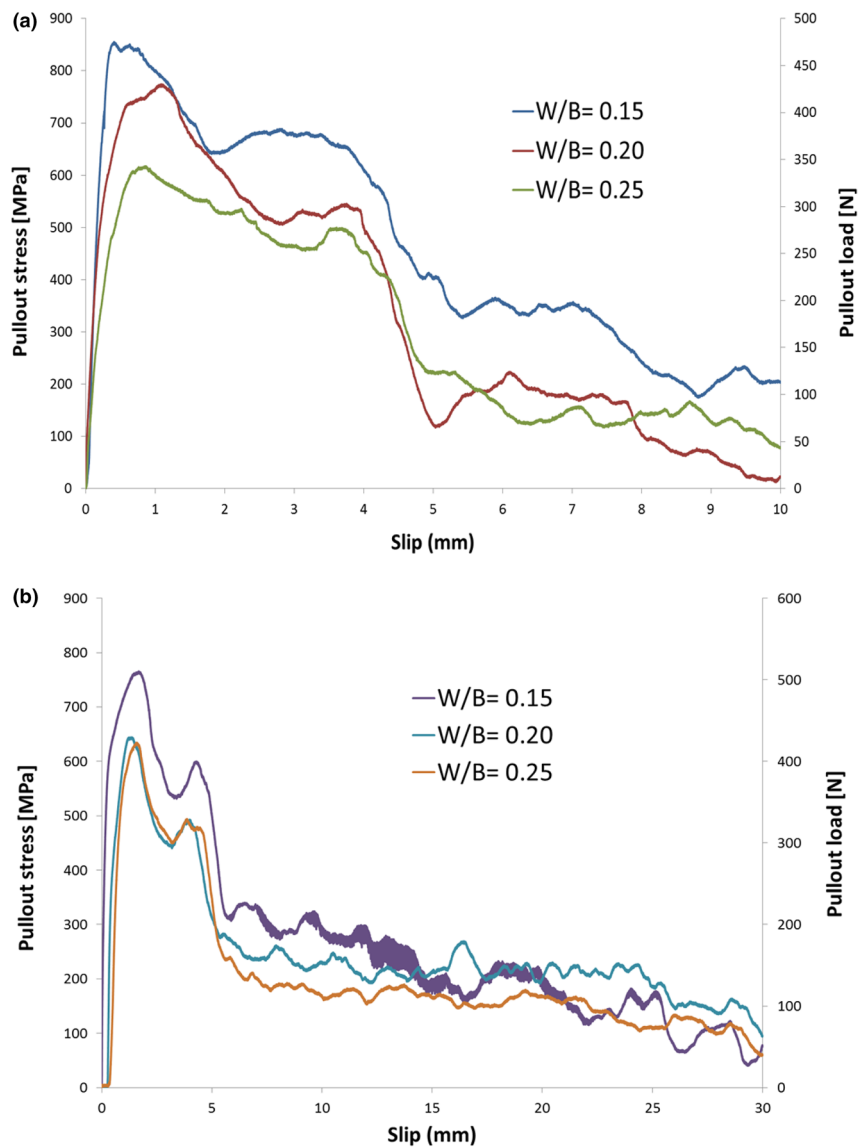
Fig. 7 Average pullout load-slip curves of 3DH2 fibres. **a** embedded length (10 mm), **b** embedded length (30 mm).

17–20, 37–47, and 43–53%, while, the corresponding decrease in the total pullout work is 6–16, 4–20, 37–46, and 38–49%, respectively.

According to Fig. 8, it can be seen that the average and equivalent bond strength are remarkably increase due to the decrease in W/B ratio. However, the great effect of decreasing W/B ratio is found to be optimal at the W/B ratio of 0.15, which has the highest values for both the average and equivalent bond strength. The significant enhancement in bond strength due to a decrease in W/B ratio from 0.25 to 0.15 may help to explain the noticeably high values of pullout load and total pullout work. For the 3DH2 fibre with embedded length of 10 mm, the average and equivalent bond strength are increased by 38.84 and 52.28%, respectively, whereas for the 3DH1 fibre it only increased by 25.83 and 16.82%, respectively, when W/B ratio decreased from 0.25 to 0.15.

Figure 9 shows the images of fibres after pullout tests with various W/B ratios. It can be seen that the end hook of both types of fibres was somehow straightened, with those pulled out from the matrix with the W/B ratio of 0.15 being more straight compared with those in matrix with other W/B ratios. The reason for this behaviour may be explained by the enhancement of the fibre-matrix interfacial properties. This was also confirmed by the remarkable improvement in pullout behaviour, equivalent bond strength and average bond strength (Table 4). Although the fibres embedded in the matrix with 0.20 and 0.25 W/B ratios were completely deformed, the full straightening of their end hook did not occur. Nevertheless, the straightening of the end hook of both types of fibres embedded in matrixes with 0.20 and 0.25 W/B ratios are similar. This reinforces the conclusions that the decreasing W/B ratio from 0.25 to 0.20 may not improve the interfacial bond characteristics as in case of 0.15 W/B.

The tensile stress induced in fibre or the maximum fibre stress is then interpreted and summarized in Table 4 and Figs. 6 and 7. Although the values of induced stress in both types of fibres are comparable in matrixes with 0.20 and 0.25 W/B ratios, a significant improvement in the maximum

Table 4 The experimental parameters of pullout test.

Series	Medium	Embedded length(mm)	P_{max} (N)	Δ_{peak} (mm)	W_{total} (N/mm)	σ_{max}/f_y (−)	σ_{max}	τ_{eq} (N/mm^2)	τ_{av}
3DH1-U1-LE10		10	216	0.61	753	0.67	909	8.72	12.51
3DH1-U1-LE15	UHPM1	15	233	1.02	1153	0.73	980	5.93	8.90
3DH2-U1-LE10		10	475	0.40	2595	0.64	747	18.36	16.85
3DH2-U1-LE30		30	510	1.67	5443	0.69	802	4.28	12.14
3DH1-U2-LE10		10	196	0.48	664	0.61	825	7.69	11.33
3DH1-U2-LE15	UHPM2	15	195	0.85	922	0.61	821	4.74	7.58
3DH2-U2-LE10		10	430	1.08	1848	0.58	676	13.08	15.29
3DH2-U2-LE30		30	429	1.36	5027	0.58	675	3.95	10.16
3DH1-U3-LE10		10	185	0.49	598	0.58	779	6.93	10.77
3DH1-U3-LE15	UHPM3	15	204	0.73	908	0.63	860	4.67	7.82
3DH2-U3-LE10		10	342	0.86	1706	0.46	539	12.07	12.14
3DH2-U3-LE30		30	423	1.58	4120	0.57	665	3.23	9.95

fibre stress was achieved for all fibres in matrix with 0.15 W/B ratio. The maximum fibre stress of the 3DH2 fibre with embedded length of 10 mm is increased by 25.41%, while for the 3DH1 fibre only 5.90% when W/B ratio decreases from 0.25 to 0.20. However, a further decrease in W/B ratio to 0.15 leads to remarkable increase in the maximum tensile stress about 38.58, and 16.68% for the 3DH2 and 3DH1 fibres, respectively. This represents an utilisation of about 64 and 67% of extra tensile capacity of these fibres, respectively.

3.3 Effect of Fibre Embedment Length on Pullout Behaviour

In order to evaluate the influence of embedment length of hooked end steel fibres on pullout behaviour, two different embedded lengths (L_E) for each type of fibres have been considered in this study. For the 3DH1 fibre, the embedment length investigated is 10 and 15 mm, while that for the 3DH2 fibre is 10 and 30 mm.

Overall, both types of fibres showed extremely similar pullout behaviour but difference in maximum pullout load and pullout work (Figs. 6, 7). It is apparent that the increase of embedment length has no great effect on the maximum pullout load but it relatively increases the total pullout work. This can be explained by the slightly higher maximum pullout load was observed for both types of fibres in 0.20 W/B ratio series with an embedded length of 10 mm than those of 15 and 30 mm (Table 4). This is also in accordance with the results of other researchers (Markovic 2006; Van Gysel 2000).

On the other hand, since the measured lengths ($L_1 + L_2$) of the end hook of the 3DH1 and 3DH2 fibres were approximately 4.80 and 5 mm (Table 2), respectively. It is believed that an embedment length of 10 mm which is roughly twice of the length of the end hook is efficient to achieve full mobilization and straightened end hook. This indicates that the pullout behaviour is drastically governed by the hook component and increasing in embedment length does not have significant contribution to the maximum pullout load. On the basis of this, it can be concluded that if the fibre is fully deformed and straightened, it seems that the fibres with a shorter embedded length (10 mm) can be used to obtain the same efficiency as fibres with a larger embedded length (15 or 30 mm). This was also confirmed from the results of average and equivalent bond strength in Table 3. Although the bond strength is drastically enhanced
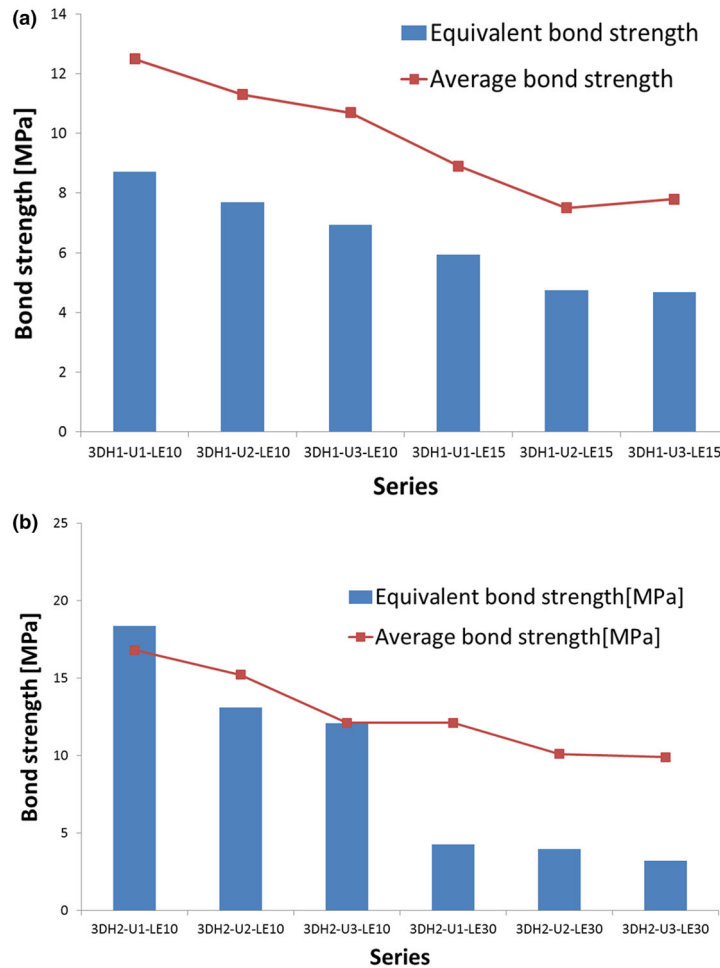
Fig. 8 Effect of W/B ratio on the bond strength of **a** 3DH1 fibres, **b** 3DH2 fibres.

by W/B ratio, the increase in fibre embedment length remarkably decreases both the average and equivalent strength. In addition, there is nearly no significant increase in the maximum pullout load relative to the increase in embedded length which leads to decrease the bond strength. It seems that the maximum pullout load significantly influenced by the plastic deformation of the fibre hook and increase the embedded length only enhances the frictional pullout stage.

Table 4 also summarizes the key parameters of pullout behaviour of all series of tests performed in this study. It can be observed that the maximum fibre stress of the 3DH1 fibres is somewhat higher than that generated by the 3DH2 fibres. On the other hand, although reducing W/B ratio particularly from 0.25 to 0.15 considerably enhances the fibres stress-slip behaviour, the increase in embedded length has no remarkable effect on the maximum fibre stress. It is noteworthy from Table 4 that for the matrix with 0.20 W/B ratio the increase in embedded length of both types of fibres did not improve fibre stress and the values of the maximum fibre stress is found to be very similar.

In comparing the pullout behaviour of 3DH1 fibre with an embedded length of 10 mm (Fig. 6a) with that of 15 mm (Fig. 6b) embedded length, no clear difference is observed, particularly, for the matrix of W/B ratio of 0.20 or 0.25.

Similarly the 3DH2 fibre showed that the increase in the embedded length from 10 to 30 mm slightly enhancing the maximum fibre stress (Fig. 7). This leads to the conclusion that the increase in fibre embedment length after specific limit which is 10 mm in this study does not contribute to maximum fibre stress but only improve the total pullout work. Although many studies reported that increase the embedded length of straight fibres can develop higher tensile stresses during pullout, it appears not to be the case for hooked-end steel fibres (Markovic 2006). Since the embedded length of 10 mm seems to be enough for achieving the full deformation and straightening of the hook, an increase of embedded length is no longer play an important role for maximum fibre stress. This behaviour was also confirmed from the results (Table 4) of the fibre efficiency ratio (σ_{max}/f_y), which represents the maximum tensile stress induced during pullout, σ_{max} over the fibre tensile strength, f_y. A slight difference is also observed between the values of (σ_{max}/f_y) ratio when the embedded length increases. Although the increase in embedded length slightly increases the maximum tensile stress induced by fibres, both types of fibres embedded in the matrix with 0.20 W/B showed the same value of (σ_{max}/f_y) ratio even with embedded length increases from 10 to 15 and 30 mm. These results strongly proved that the end hook of fibres with embedded
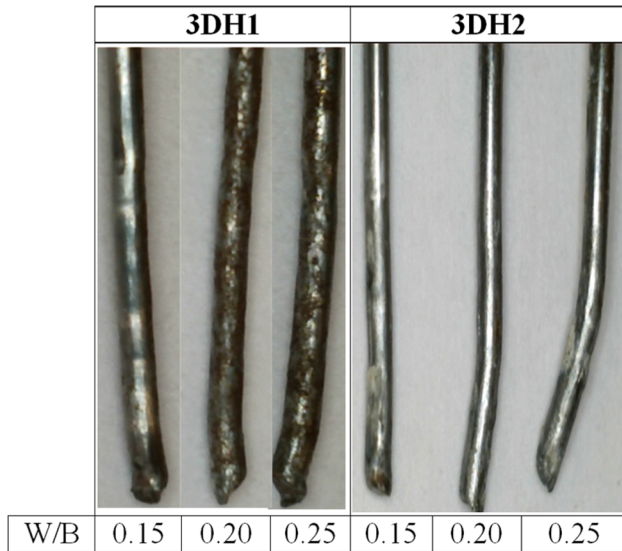
	3DH1			3DH2		
W/B	0.15	0.20	0.25	0.15	0.20	0.25

Fig. 9 Image shows the comparison between 3DH1 and 3DH2 fibres after pullout.

length of 10 mm can be fully deformed and straightened, and any increase in the embedded length does not affect much the pullout behaviour.

3.4 Microscopic Observations (SEM—Scanning Electron Microscopy)

Figure 10a shows SEM images of the steel fibre-matrix interface of the UHPM1 mixture (W/B = 0.15). It can be seen from this figure that the particle dispersion and packing density at fibre-matrix interface is well-developed in the UHPM1 matrix. This is mainly due to the low W/B and pozzolanic reactions between silica fume and calcium hydroxide (CH), which consumes most of the CH crystals and transforms them to C–S–H (Shi et al. 2015; Chan and Chu 2004). The densification of microstructures in the ITZ due to congestion of the hydration products significantly enhances the bond properties between fibre and matrix. (Lee and Jacobsen 2011) found that mortar with 0.3 W/B had higher debonding loads and fracture energies than that of the 0.5 W/B. It has been reported that the incorporation of silica fume can effectively improve the interfacial bond by reducing the porosity, refining the pores, and increasing the density and content of the C–S–H (Zeng et al. 2012; Abu-Lebdeh et al. 2011). Also, the lower the porosity, the higher is the particle packing density in the ITZ and bulk the matrix.

Thus, a higher content of the cement hydration products such as C–S–H which are important to enhance the microstructure and microhardness of the ITZ, resulting in improves the transmission of stress between the fibre and matrix (Wu et al. 2016).

Figure 10b shows the SEM images of the fibre-matrix interface of the UHPM2 mixture (W/B = 0.20). It can be observed from this figure that some pores are formed in the ITZ. A according to (Lee and Jacobsen 2011), although the incorporation of 10% silica fume has a positive effect on the fracture and compressive energies, the improvement in debonding loads was not observed. They revealed that if silica fume particle is not dispersed properly in the mortar, an increased amount of C–S–H through the pozzolanic reaction cannot be achieved, regardless of W/B. With further increase in W/B from 0.20 to 0.25, a numerous small and large pores were observed which have formed along the ITZ (Fig. 10c). Basically, higher water content is responsible for forming the pores, ultimately leads to decrease the bond strength of the UHPM3 mixture significantly. (Wu et al. 2016) has also observed a large porous zone located within 50 mm from the fibre edge for UHPM with 0.18 W/B. This weak zone could significantly reduce the contact surface area between fibre and matrix. These facts may help to explain the relatively lower pull out load and total pull-out work of the matrix with 0.25 W/B ratio compared with 0.15 W/B.

3.5 Mechanical Anchorage Contribution of the End Hook to Pullout Behaviour

To get better understanding of the contribution provided by the end hook to pullout behaviour, a quantitative account for hook mechanisms has been adopted. This follows that the proposed procedure is mainly dependent on the measured hook lengths which are approximately 4.78 and 5 mm for the 3DH1 and 3DH2 fibres respectively (Table 2). As can be seen from Fig. 11, the end hook contribution is nearly being finished at 4.78 mm for the 3DH1 fibre and 5 mm for the 3DH2 fibre, which corresponds to decay of pullout load due to complete deformation and straightening of the end hook. Consecutively, the friction resistance contribution initiates and continues until fibres completely pullout. On the other hand, while test results revealed that the debonding process finishes at fibre slips up to less than 0.1 mm; its contribution to total pullout work is found to be lower than 1% for all fibres series. Therefore, the contribution due to debonding process can be neglected. This procedure
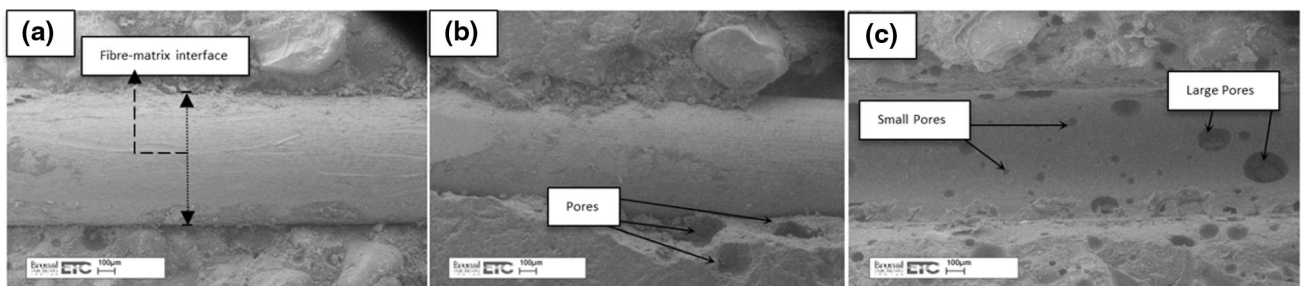

Fig. 10 SEM images of the fibre-matrix interface. **a** UHPM1(W/B = 0.15), **b** UHPM2 (W/B = 0.20) and **c** UHPM3 (W/B = 0.25).
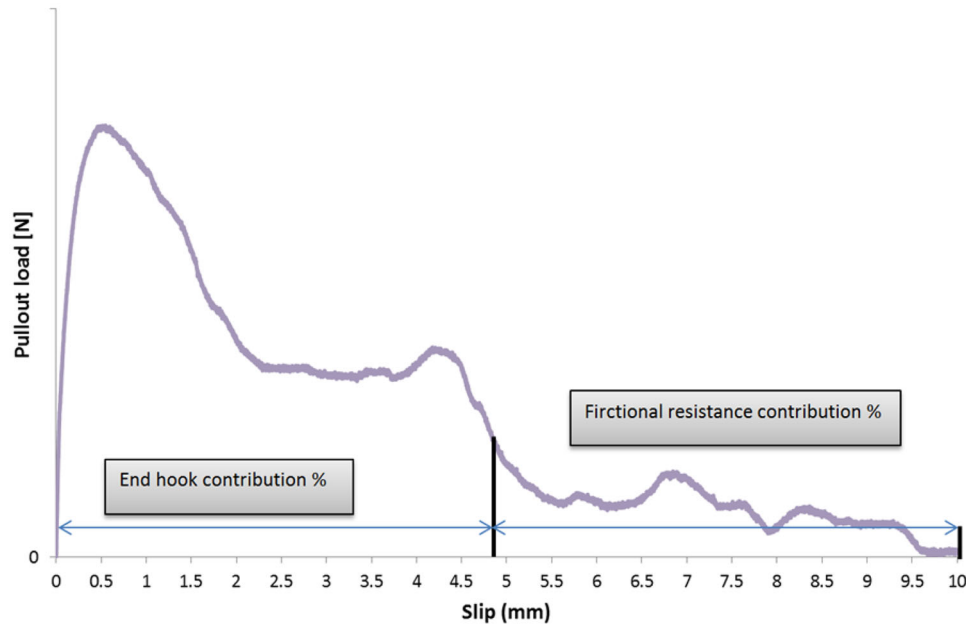
Fig. 11 Example showing the contribution of the end hooks component and frictional resistance to the overall pullout behaviour of 3DH2 fibres.

provides basic information about the effects of the parameters such as W/B ratio, diameter, embedded length and tensile strength of fibres on pullout behaviour.

The percentage contribution of the end hook and frictional resistance on the total pullout work is summarized in Table 5. From the experimental results of the both types of hooked fibres (Table 5), it can be observed that as the embedded length of fibre increases, the percentage of hook contribution in terms of total pullout work dramatically decreases. Although the percentage of hook contribution with embedded length of 10 mm is significantly higher than that of the frictional resistance, the increase in embedded

length especially of the 3DH2 fibres drastically increase the contribution percentage of frictional resistance. The increase of embedded length of the 3DH1 fibres from 10 to 15 mm leads to slight decrease in the hook contribution, while for the 3DH2 fibres the increase in embedded length from 10 to 30 mm results in a sharp decrease in hook contribution up to half of that in case of 10 mm embedded length. This can be attributed to large surface area of fibre in contact with surrounding matrix which increases the frictional resistance to pullout. Based on experimental results, it appears that the embedded length has a greater effect on total pullout work than maximum pullout load.

Table 5 The end hook and frictional resistance contribution to the total pullout work.

| Series	Medium	Embedded length(mm)	End hook contribution %	Frictional resistance contribution %
3DH1-U1-LE10		10	82.42	17.57
3DH1-U1-LE15	UHPM1	15	64.02	35.97
3DH2-U1-LE10		10	69.47	30.52
3DH2-U1-LE30		30	37.64	62.35
3DH1-U2-LE10		10	83.67	16.32
3DH1-U2-LE15	UHPM2	15	68.46	31.53
3DH2-U2-LE10		10	80.88	19.11
3DH2-U2-LE30		30	30.43	69.56
3DH1-U3-LE10		10	83.47	16.52
3DH1-U3-LE15	UHPM3	15	70.48	29.51
3DH2-U3-LE10		10	76.36	23.63
3DH2-U3-LE30		30	36.31	63.68
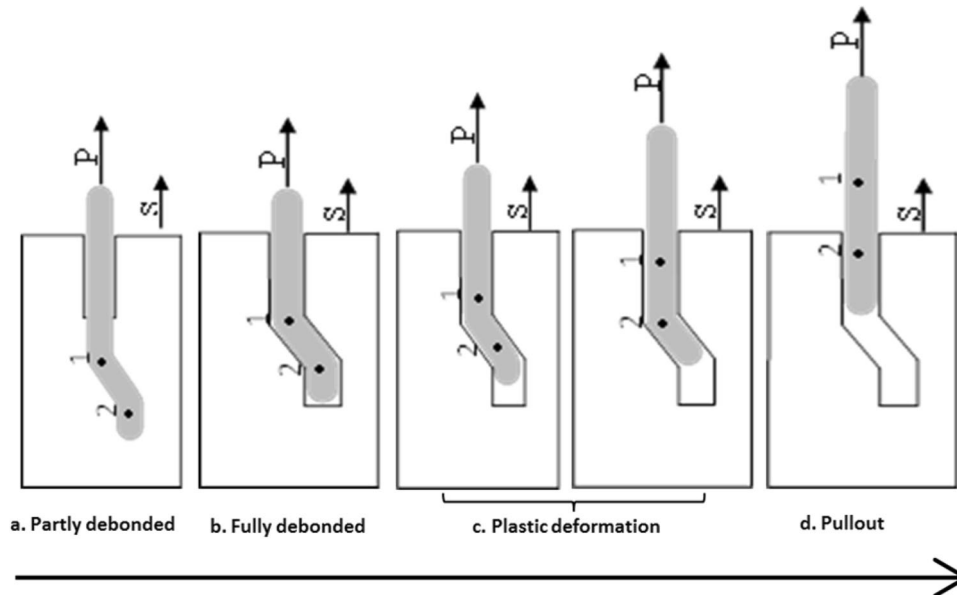
Fig. 12 Pullout process of a hooked end steel fibre.

3.6 Difference in the Pullout Behaviour of Two Hooked End Fibres

The observed pullout load-slip curves of hooked end steel fibres embedded in UHPM is generally characterised by a steady increase up to peak load as a result of the combination of two mechanisms which are: detachment of the fibre-matrix bond and mechanical anchorage of the end hook. Once the fibre-matrix bond is fully detached, two plastic hinges of the fibre hook undergo cold work causing deformation and bending of the end hook (Alwan et al. 1999), in Fig. 12, the two plastic hinges are identified as 1 and 2. As a result of deformation and slippage of the first plastic hinge a sharp decrease in pullout load takes place. Nevertheless, initial increase in pullout load can be observed due to the progressive deformation of the second plastic hinge in conjunction with straightening of the end hook. The last stage of the pullout will occur under sliding friction until complete pullout of fibre from the mortar matrix.

The comparison of the pullout behaviour between the two hooked end fibres shows that the maximum pullout load of the 3DH2 fibres is approximately more than two times that of the 3DH1 fibres for all W/B ratios. Moreover, the total pullout work of the 3DH2 fibres embedded up to half fibre length ($L_E = 30$ mm) is roughly five times that the 3DH1 fibres ($L_E = 15$ mm). It is believed that the reason for the enhanced pullout work is due to the increased embedded length which leads to large surface area of fibre in contact with surrounding matrix. Note that the embedded length of the 3DH2 fibre ($L_E = 30$ mm) is two times that of the 3DH1 fibre ($L_E = 15$ mm), to allow fair comparison an embedment length of 10 mm for both types of fibres is considered here. The pullout work of the 3DH2 fibre is also approximately three times greater than that of the 3DH1 fibre. This may be attributed to the fibre diameter that increases the bending stiffness of fibre hook, because more energy is required during the pullout process.

On the other hand, although the decrease in W/B ratio has positive effect for both types of fibres, this effect is more pronounced for the 3DH2 (diameter of 0.9 mm) than that of the 3DH1 (diameter of 0.55 mm) fibre. The reduction of W/B ratio from 0.25 to 0.15 leads to increases in maximum pullout load of the 3DH2 is 38.88%, which is approximately more than two times that achieved by the 3DH1 fibres (16.75%). These results suggest that the fibre with larger diameter is considerably influenced by enhancing fibre-matrix interfacial properties than that with smaller diameter.

For the fibre stress-slip, the induced stress in the 3DH1 fibres which have smaller fibre diameter ($d_{f} = 0.55$), is higher than that of the 3DH2 fibres with ($d_{f} = 0.90$) (Fig. 12). This may be due to the larger cross-sectional area of the 3DH2 fibre which is approximately 2.6 times greater than that of the 3DH1 fibre. The maximum tensile stress induced in the 3DH1 fibres with the embedded length of 10 mm is higher by 21.68, 22.11 and 44.52% than those in the 3DH2 fibres for 0.15, 0.20 and 0.25 W/B ratio, respectively. Despite the fact that the tensile strength of the 3DH1 fibres ($f_y = 1345$ MPa) is higher than that of the 3DH2 fibres ($f_y = 1160$ MPa), a slight difference in the values of (σ_{max}/f_y) ratio were observed. This indicates that the 3DH2 and 3DH1 fibres have somewhat similar efficiency in the utilization of tensile strength capacity.

4. Conclusions

The effect of W/B ratio of ultra-high performance mortar on pullout behaviour of two types of hooked end steel fibres has been investigated. Based on experimental results, the following conclusions can be drawn:

1. The maximum pullout load of the 3DH2 fibres was more than two times that of the 3DH1 fibres. In

addition, in case of the same embedded length the total pullout work of the 3DH2 fibres was about three times that of the 3DH1 fibres.

2. For the same fibre geometry, an increase in embedded length had no appreciable effect on the maximum pullout load but resulted in a slight improvement in the total pullout work due to larger surface area of fibre in contact with surrounding matrix. The little effect of fibre embedded length on bond properties is due to very limited difference in length and significant mechanical anchorage associated with hooked end.

3. The decrease in W/B ratio from 0.2 to 0.15 had a significant effect on the overall pullout behaviour. However, no remarkable contribution could be observed when W/B ratio decreased from 0.25 to 0.20. The hooked end fibres with larger diameter would be a better choice with lower W/B ratio.

4. For the same embedded length, the equivalent bond strength of the 3DH2 fibres was approximately two times greater than that of the 3DH1 fibres for all series.

5. Though the tensile strength of the 3DH1 fibres was higher by 16% than that of the 3DH2 fibres, both fibres showed similar efficiency of utilising its tensile stress capacity. The mechanical contribution of the 3DH2 fibres would be highly effective if the fibre tensile strength can be increased.

Acknowledgements

Open Access

References

Abbas, S., Nehdi, M., & Saleem, M. (2016). Ultra-high performance concrete: Mechanical performance, durability, sustainability and implementation challenges. *International Journal of Concrete Structures and Materials, 10*(3), 271–295.

Abdallah, S., Fan, M., & Rees, D. W. A. (2016a). Analysis and modelling of mechanical anchorage of 4D/5D hooked end steel fibres. *Materials and Design, 112,* 539–552.

Abdallah, S., Fan, M., & Zhou, X. (2016b). Effect of hooked-end steel fibres geometry on pull-out behaviour of ultra-high performance concrete. *World Academy of Science, Engineering and Technology, International Journal of Civil, Environmental, Structural, Construction and Architectural Engineering, 10*(12), 1530–1535.

Abdallah, S., Fan, M., Zhou, X., & Geyt, S. (2016c). Anchorage effects of various steel fibre architectures for concrete reinforcement. *International Journal of Concrete Structures and Materials, 10,* 325–335.

Abu-Lebdeh, T., Hamoush, S., Heard, W., & Zornig, B. (2011). Effect of matrix strength on pullout behavior of steel fiber reinforced very-high strength concrete composites. *Construction and Building Materials, 25*(1), 39–46.

Adjrad, A., Bouafia, Y., Kachi, M., & Ghazi, F. (2016). Prediction of the rupture of circular sections of reinforced concrete and fiber reinforced concrete. *International Journal of Concrete Structures and Materials, 1,* 373–381.

Alberti, M. G., Enfedaque, A., Gálvez, J. C., Cánovas, M. F., & Osorio, I. R. (2014). Polyolefin fiber-reinforced concrete enhanced with steel-hooked fibers in low proportions. *Materials and Design, 60,* 57–65.

Alwan, J. M., Naaman, A. E., & Guerrero, P. (1999). Effect of mechanical clamping on the pull-out response of hooked steel fibers embedded in cementitious matrices. *Concrete Science and Engineering, 1*(1), 15–25.

Beglarigale, A., & Yazıcı, H. (2015). Pull-out behavior of steel fiber embedded in flowable RPC and ordinary mortar. *Construction and Building Materials, 75,* 255–265.

Bentur, A., Wu, S., Banthia, N., Baggott, R., Hansen, W., Katz, A., Leung, C., Li, V., Mobasher, B., & Naaman, A. (1995). Fiber-matrix interfaces. In A. Naaman & Reinhardt H. (Eds.), *Chapter 5 van pre-proceedings 2nd international workshop high performance fiber reinforced cement composites (HPF-RCC-95), 11–14 juni* (pp. 139–182). Ann Arbor, MI, USA.

Beygi, M. H. A., Kazemi, M. T., Nikbin, I. M., & Amiri, J. V. (2013). The effect of water to cement ratio on fracture parameters and brittleness of self-compacting concrete. *Materials and Design, 50,* 267–276.

Chan, Y., & Chu, S. (2004). Effect of silica fume on steel fiber bond characteristics in reactive powder concrete. *Cement and Concrete Research, 34*(7), 1167–1172.

Chan, Y., & Li, V. C. (1997). Effects of transition zone densification on fiber/cement paste bond strength improvement. *Advanced Cement Based Materials, 5*(1), 8–17.

Cunha, V. M. (2010). Steel fibre reinforced self-compacting concrete (from micromechanics to composite behavior).

Deeb, R., Ghanbari, A., & Karihaloo, B. L. (2012). Development of self-compacting high and ultra high performance concretes with and without steel fibres. *Cement & Concrete Composites, 34*(2), 185–190.

Dinh, N., Choi, K., & Kim, H. (2016). Mechanical properties and modeling of amorphous metallic fiber-reinforced concrete in compression. *International Journal of Concrete Structures and Materials, 10,* 221–236.

El-Mal, H. A., Sherbini, A., & Sallam, H. (2015). Mode II fracture toughness of hybrid FRCs. *International Journal of Concrete Structures and Materials, 9*(4), 475–486.

EN, B. 12350-8. (2010). Testing fresh concrete. *Self-compacting concrete. Slump-flow test.*

Hwang, J., Lee, D. H., Ju, H., Kim, K. S., Kang, T. H., & Pan, Z. (2016). Shear deformation of steel fiber-reinforced

prestressed concrete beams. *International Journal of Concrete Structures and Materials, 10*(3), 53–63.

Islam, M. S., & Alam, S. (2013). Principal component and multiple regression analysis for steel fiber reinforced concrete (SFRC) beams. *International Journal of Concrete Structures and Materials, 7*(4), 303–317.

Joo Kim, D. (2009). *Strain rate effect on high performance fiber reinforced cementitious composites using slip hardening high strength deformed steel fibers.* ProQuest.

Kang, S., Lee, K., Choi, J., Lee, Y., Felekoğlu, B., & Lee, B. Y. (2016). Control of tensile behavior of ultra-high performance concrete through artificial flaws and fiber hybridization. *International Journal of Concrete Structures and Materials, 10*(3), 33–41.

Laranjeira de Oliveira, F. (2010). Design-oriented constitutive model for steel fiber reinforced concrete. *Unpublished doctoral dissertation. Universitat Politècnica de Catalunya, Spain.*

Lee, S. F., & Jacobsen, S. (2011). Study of interfacial microstructure, fracture energy, compressive energy and debonding load of steel fiber-reinforced mortar. *Materials and Structures, 44*(8), 1451–1465.

Lee, Y., Kang, S., & Kim, J. (2010). Pullout behavior of inclined steel fiber in an ultra-high strength cementitious matrix. *Construction and Building Materials, 24*(10), 2030–2041.

Li, H., & Liu, G. (2016). Tensile properties of hybrid fiber-reinforced reactive powder concrete after exposure to elevated temperatures. *International Journal of Concrete Structures and Materials, 10,* 29–37.

Lim, W., & Hong, S. (2016). Shear tests for ultra-high performance fiber reinforced concrete (UHPFRC) beams with shear reinforcement. *International Journal of Concrete Structures and Materials, 10,* 177–188.

Lu, L., Tadepalli, P., Mo, Y., & Hsu, T. (2016). Simulation of prestressed steel fiber concrete beams subjected to shear. *International Journal of Concrete Structures and Materials, 10*(3), 297–306.

Markovic, I. (2006). *High-performance hybrid-fibre concrete: Development and utilisation.* Delft: IOS Press.

Petrone, F., Shan, L., & Kunnath, S. K. (2016). Modeling of RC frame buildings for progressive collapse analysis. *International Journal of Concrete Structures and Materials, 10*(1), 1–13.

Romualdi, J. P., Ramey, M., & Sanday, S. C. (1968). Prevention and control of cracking by use of short random fibers. *Special Publication, 20,* 179–204.

Shaikh, F. U. A., Shafaei, Y., & Sarker, P. K. (2016). Effect of nano and micro-silica on bond behaviour of steel and polypropylene fibres in high volume fly ash mortar. *Construction and Building Materials, 115,* 690–698.

Shi, C., Wu, Z., Xiao, J., Wang, D., Huang, Z., & Fang, Z. (2015). A review on ultra high performance concrete: Part I. Raw materials and mixture design. *Construction and Building Materials, 101,* 741–751.

Sorensen, C., Berge, E., & Nikolaisen, E. B. (2014). Investigation of fiber distribution in concrete batches discharged from ready-mix truck. *International Journal of Concrete Structures and Materials, 8*(4), 279–287.

Srikar, G., Anand, G., & Prakash, S. S. (2016). A study on residual compression behavior of structural fiber reinforced concrete exposed to moderate temperature using digital image correlation. *International Journal of Concrete Structures and Materials, 10,* 75–85.

Tadepalli, P. R., Dhonde, H. B., Mo, Y., & Hsu, T. T. (2015). Shear strength of prestressed steel fiber concrete I-beams. *International Journal of Concrete Structures and Materials, 9*(3), 267–281.

Torregrosa, C. E. E. (2014). *Dosage optimization and bolted connections for UHPFRC ties.*

Van Gysel, A. (2000). Studie van het uittrekgedrag van staalvezels ingebed in een cementgebonden matrix met toepassing op staalvezelbeton onderworpen aan buiging. Published.

Wang, D., Shi, C., Wu, Z., Xiao, J., Huang, Z., & Fang, Z. (2015). A review on ultra high performance concrete: Part II. Hydration, microstructure and properties. *Construction and Building Materials, 96,* 368–377.

Wille, K., El-Tawil, S., & Naaman, A. E. (2014). Properties of strain hardening ultra high performance fiber reinforced concrete (UHP-FRC) under direct tensile loading. *Cement & Concrete Composites, 48,* 53–66.

Wille, K., & Naaman, A. (2010). Bond stress-slip behavior of steel fibers embedded in ultra high performance concrete. *Proceedings of 18th European conference on fracture and damage of advanced fiber-reinforced cement-based materials* (99–111).

Wille, K., & Naaman, A. E. (2012). Pullout behavior of high-strength steel fibers embedded in ultra-high-performance concrete. *ACI Materials Journal, 109*(4), 479–588.

Wille, K., & Naaman, A. E. (2013). Effect of ultra-high-performance concrete on pullout behavior of high-strength brass-coated straight steel fibers. *ACI Materials Journal, 110*(4), 451–462.

Wu, Z., Shi, C., He, W., & Wu, L. (2016a). Effects of steel fiber content and shape on mechanical properties of ultra high performance concrete. *Construction and Building Materials, 103,* 8–14.

Wu, Z., Shi, C., & Khayat, K. H. (2016b). Influence of silica fume content on microstructure development and bond to steel fiber in ultra-high strength cement-based materials (UHSC). *Cement & Concrete Composites, 71,* 97–109.

Yoo, D., & Yoon, Y. (2016). A review on structural behavior, design, and application of ultra-high-performance fiber-reinforced concrete. *International Journal of Concrete Structures and Materials, 10,* 125–142.

Zeng, Q., Li, K., Fen-chong, T., & Dangla, P. (2012). Pore structure characterization of cement pastes blended with high-volume fly-ash. *Cement and Concrete Research, 42*(1), 194–204.